Catal Lett (2011) 141:939–947
DOI 10.1007/s10562-011-0640-0

Study of the Alkylation of Phenol with Methanol on Zn(H)-Exchanged NaY Zeolites

L. F. González Peña · M. E. Sad · C. L. Padró · C. R. Apesteguía

Received: 17 March 2011 / Accepted: 30 May 2011 / Published online: 10 June 2011

Abstract The gas-phase alkylation of phenol with methanol was studied at 473 K on zeolite NaY exchanged with Zn^{+2} (samples Zn(*x*)NaY) or H^+ (samples Na(*x*)HY) cations. Zeolite NaY contained only weak and medium Lewis acid sites. The addition of Zn^{+2} formed essentially strong Lewis acid sites. In contrast, the exchange of NaY with H^+ generated Brønsted acid sites and decreased the density of Lewis acid sites. Zeolite NaY was inactive at 473 K, but after its exchange with Zn^{2+} efficiently promoted the phenol methylation reaction. Phenol conversion and the selectivities to *o*- and *p*-cresols increased with the Zn content in the sample. The exchange of Na^+ with H^+ also activated the parent NaY zeolite. At similar phenol conversion levels, Na(*x*)HY samples formed more anisole and less cresols than Zn(*x*)NaY. All the Zn(*x*)NaY and Na(*x*)HY samples deactivated on stream, but the catalyst activity decay increased with the exchange degree.

Keywords Phenol methylation · Zeolites Zn(*x*)NaY · Zeolites Na(*x*)HY · Alkylation reactions · Zeolite NaY

1 Introduction

The gas-phase alkylation of phenol with methanol produces valuable chemicals such as cresols, anisole, and polyalkylated phenols. In particular, cresol isomers (*m*-, *p*-, and *o*-cresols) are widely employed for the synthesis of pharmaceuticals, herbicides, antioxidants, agrochemicals and dyes [1–4]. The direct attack of methanol to phenol produces anisole by *O*-alkylation, and cresols by *C*-alkylation; then, the consecutive alkylation of anisole and cresol isomers form methylanisoles and xylenols, respectively (Scheme 1). Previous work has shown that the catalyst activity and selectivity depend on the surface acid–base properties. Solid bases, in particular MgO, selectively alkylate phenol in *ortho*-position, producing essentially *o*-cresol and 2,6 xylenol [5, 6]. Solid acids such as silica-alumina, Nafion-H resin, HPA/SiO_2, and zeolites HBEA and HY, convert phenol to a mixture of anisole, cresols, xylenols and methylanisoles [7–13]. Brønsted solid acids promote the *O*-alkylation of phenol [10, 11] while Lewis solid acids (SiO_2–Al_2O_3) and zeolites containing similar amounts of Lewis and Brønsted acid sites (HBEA, HY) favor the *C*-alkylation of phenol [7, 14]. In spite of all these studies, knowledge on the reaction pathways leading from phenol to cresol isomers and on the exact requirements of density, nature and strength of surface acid sites for improving the cresol yield and selectivity on solid acids is still needed.

In a previous paper [15], we studied the gas-phase alkylation of phenol with methanol on different solid acids, namely HPA/SiO_2, zeolites HZSM5, HBEA and HY, SiO_2–Al_2O_3 and Al-MCM-41. We found that the catalyst activity, selectivity and stability for producing cresols from phenol alkylation greatly depend on the pore microstructure and the nature, density and strength of surface acid sites. In this work we investigated further the methylation of phenol on acid zeolites with the aim of ascertaining the effect of the nature and strength of surface acid sites on promoting the primary and secondary pathways involved in the reaction network. Specifically, we exchanged a

L. F. González Peña · M. E. Sad · C. L. Padró · C. R. Apesteguía (✉)
Catalysis Science and Engineering Research Group (GICIC), INCAPE, (UNL-CONICET), Santiago del Estero 2654, 3000 Santa Fe, Argentina
e-mail: capesteg@fiq.unl.edu.ar
URL: http://www.fiq.unl.edu.ar/gicic

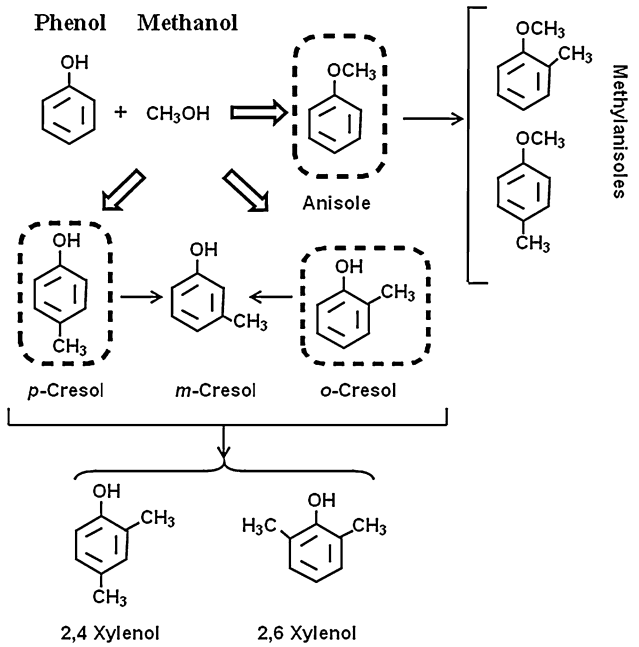

Scheme 1 Simplified reaction network for the alkylation of phenol with methanol

commercial NaY zeolite with increasing amounts of Zn^{+2} or H^+ cations in order to increase the density and strength of acid sites and regulate the Lewis/Brønsted acid sites ratio. Results showed that the addition of Zn^{+2} cations to zeolite NaY increases the density and strength of surface Lewis acid sites; as a consequence, the selectivity to cresols increased with the Zn content in the sample at the expenses of anisole, reaching up to about 63% cresols. In contrast, the exchange of zeolite NaY with H^+ cations formed essentially Brønsted acid sites that initially promotes the preferential formation of anisole and the *ortho*-selectivity, producing more *o*-cresol than *p*-cresol. All the samples deactivated on stream, but the activity decay was particularly significant on catalysts containing a high density of strong Brønsted acid sites.

2 Experimental

2.1 Catalyst Preparation

Zeolite NaY was a commercial zeolite (UOP-Y 54, Si/Al = 2.4) of 700 m^2/g. Zeolites Zn(2.4)NaY, Zn(5.2)NaY and Zn(9.3)NaY containing 2.4, 5.2 and 9.3% Zn, respectively, were prepared from commercial NaY by successive ion exchanges with aqueous solutions of $Zn(NO_3)_2.6H_2O$ (Riedel-de Haën, 98%) at 353 K. Zeolites Zn(2.4)NaY and Zn(5.2)NaY were prepared by performing one exchange with $Zn(NO_3)_2{\cdot}6H_2O$ solutions of 0.05 and 0.2 M, respectively; zeolite Zn(9.3)NaY was obtained by exchanging commercial NaY three times, with a 0.5 M $Zn(NO_3)_2$ solution. Zeolites Na(6.0)HY and Na(4.9)HY were obtained by single ion exchange of commercial NaY with NH_4Cl aqueous solutions (Merck, 99.8%) of 0.055 and 0.11 M, respectively, at 353 K; zeolite Na(0.3)HY was prepared by triple ion exchange with 1.5 M NH_4Cl solutions. All the exchanged samples were filtered, washed with hot distilled water, dried at 373 K for 12 h and finally calcined in air at 723 K for 3 h.

2.2 Catalyst Characterization

BET surface areas (S_g) were measured by N_2 physisorption at 77 K in a Quantochrome Corporation NOVA-1000 sorptometer. The crystal structure of the samples was determined by powder X-ray diffraction methods (XRD) using a Shimadzu XD-D1 diffractometer and Ni-filtered CuKα radiation. The diffraction patterns were scanned in the 2θ of 2°–45°. The chemical compositions were measured by atomic absorption spectroscopy.

The density and strength of the acid sites were determined by temperature programmed desorption (TPD) of NH_3 adsorbed at 373 K. Samples (100 mg) were treated in He (60 cm^3/min) at 773 K for 2 h, cooled down to 373 K, and then exposed to a 1% NH_3/He stream during 45 min. Weakly adsorbed NH_3 was removed by flushing with He at 373 K for 90 min. Finally, the sample temperature was increased at 10 K/min in a He flow of 60 cm^3/min and desorbed NH_3 was analyzed by mass spectrometry in a Baltzers Omnistar unit.

The nature of the surface acid sites was determined by Infrared Spectroscopy (IR) in a Shimadzu FTIR Prestige-21 spectrophotometer using pyridine as a probe molecule. Samples of wafers were formed by pressing 20–40 mg of the catalyst at 5 ton/cm^2 and transferred to a sample holder made of quartz. An inverted T-shaped Pyrex cell containing the sample wafer was used. The two ends of the short arm of the T were fitted with CaF_2 windows. Samples were initially outgassed in vaccum at 773 K during 2 h and then a background spectrum was recorded after cooled down to room temperature. Spectra were recorded at room temperature, after admission of pyridine, adsorption at room temperature and sequential evacuation at 423 and 573 K.

2.3 Catalytic Testing

The gas phase alkylation of phenol (Merck, >99%) with methanol (Merck, 99.8%) was carried out in a fixed bed reactor at 473 K and 101.3 kPa in continuous flow of N_2. Samples (particles with 0.35–0.42 mm diameter) were pretreated in situ, at 723 K in air flow for 2 h before reaction. Methanol (M) and phenol (P) were fed (M/P = 2:1 molar) using a syringe pump and vaporized

into flowing N_2 to give a $N_2/(P + M)$ molar ratio of 26.8. The exit gases were analyzed on-line using an Agilent 6850 chromatograph that was equipped with a flame ionization detector, temperature programmer and a 30 m Innowax column (inner diameter: 0.32 mm, film thickness: 0.5 μm). Samples were collected every 20 min during 4 h. Main reaction products were cresols (*o*-, *m*- and *p*-cresols), anisole, xylenols (dimethylphenols) and methylanisoles (MA); dimethyl ether and hydrocarbons produced by methanol dehydration were also detected.

Phenol conversion (X_P) was calculated as: $X_P = \Sigma Y_i/(\Sigma Y_i + Y_P)$, where ΣY_i is the molar fraction of products formed from phenol, and Y_P is the outlet molar fraction of phenol. The selectivity to product *i* (S_i, mol of product *i*/mol of phenol reacted) was determined as: $S_i = [Y_i/\Sigma Y_i]$.

3 Results and Discussion

3.1 Catalyst Characterization

The chemical composition, surface area and crystallinity of the samples are presented in Table 1. The Zn content in exchanged NaY zeolites increased with both the concentration of the exchange solution and the number of exchanges. The largest Zn concentration was 9.3%, sample Zn(9.3)NaY, corresponding to a Zn/Al ratio of 0.29. The amount of Na remaining on sample Zn(9.3)NaY was 0.4%, corresponding to an exchange degree of 95%. On the other hand, the triple ion exchange of zeolite NaY with a 1.5 M NH_4Cl solution diminished the Na content from 7.5% (zeolite NaY) to 0.3% (sample Na(0.3)HY); the exchange degree was 96%.

The X-ray diffractograms in Fig. 1 revealed that the crystalline structure of parent zeolite NaY did not change substantially following the ionic exchanges treatments; the crystallinity of ion-exchanged zeolites was in fact higher than 80% in all the cases (Table 1). Consistently, the surface area of zeolite NaY was not significantly affected by ionic exchange procedures; the highest surface area drop (13%) was observed for sample Zn(9.3%)NaY.

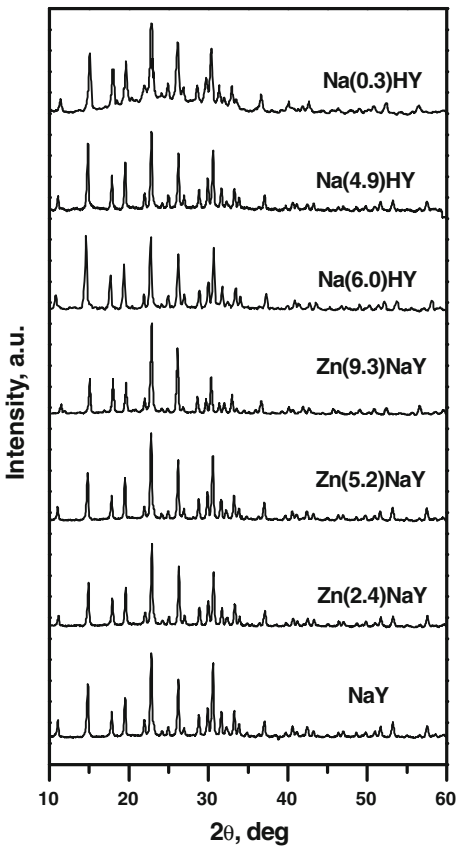

Fig. 1 XRD diffractograms of the samples

The strength and density of surface acid sites were studied by NH_3 TPD. The NH_3 desorption profiles are shown in Fig. 2a (zeolites Zn(*x*)NaY) and Fig. 2b (zeolites Na(*x*)HY). The TPD profile of NaY presented a single low-temperature asymmetric peak at about 480 K (Fig. 2a). The addition of Zn increased the low-temperature peak at 480 K and gave rise to a wide desorption band at temperatures higher than 700 K; Zn(9.30)NaY presented an additional shoulder at about 550 K. Thus, the exchange of zeolite NaY with Zn^{2+} cations not only increased the concentration of weak and medium acid sites but also generated strong acid sites. The NH_3 TPD curves of Na(*x*)HY samples in Fig. 2b displayed the low-temperature

Table 1 Chemical composition, surface area and cristallinity of the samples used in this work

Samples	Chemical composition		Surface area	Crystallinity
	Na (wt %)	Zn (wt %)	S_g (m^2/g)	(%)
NaY	7.5	–	700	84.5
Zn(2.4)NaY	5.6	2.4	673	83.8
Zn(5.2)NaY	2.9	5.2	662	83.0
Zn(9.3)NaY	0.4	9.3	612	80.4
Na(6.0)HY	6.0	–	684	94.5
Na(4.9)HY	4.9	–	670	95.6
Na(0.3)HY	0.3	–	660	97.5

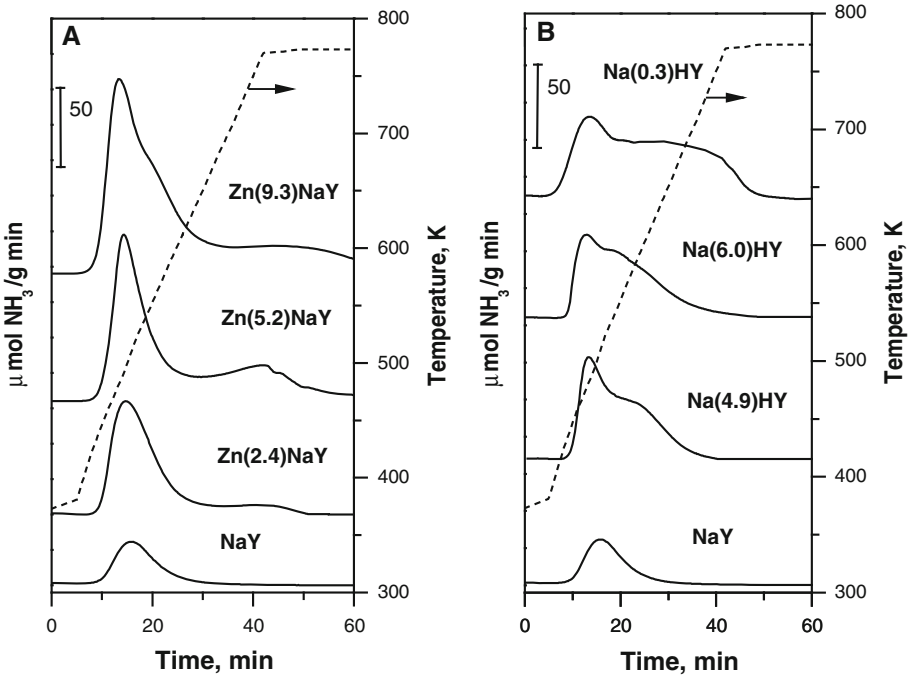

Fig. 2 TPD profiles of NH_3 on: **a** zeolites Zn(*x*)NaY; **b** zeolites Na(*x*)HY. Heating rate, 10 K/min

desorption peak at about 480 K observed for the zeolite NaY and a high-temperature band that shifted to higher temperatures with the exchange degree. Table 2 shows that the density of acid sites on zeolite Na(0.3)HY (1430 μmol/g) was significantly higher than that on zeolite Na(4.9)HY (924 μmol/g).

Figure 3 shows the FTIR spectra obtained for all the samples in the OH stretching region (3400–3800 cm^{-1}). NaY and Zn(*x*)NaY samples did not exhibit any absorption band, which revealed the absence of Brønsted acid sites on all these samples. In contrast, zeolites Na(*x*)HY showed three OH stretching bands corresponding to terminal silanols, Si–OH (3740 cm^{-1}), Si–OH–Al groups located in accessible large cavities (3640 cm^{-1}), and Si–OH–Al groups located in sodalite cage and hexagonal prisms (3550 cm^{-1}) [16]. Terminal Si–OH groups at 3743 cm^{-1} are very weak acid sites while the high-frequency Si–OH–Al groups represent the strongest Brønsted acid sites [17]. Figure 3 shows that the Brønsted acidity of zeolites Na(*x*)HY increased with the exchange degree.

The nature of surface acid sites was studied by FTIR of adsorbed pyridine. The spectra obtained after pyridine adsorption at room temperature and consecutive evacuation at 423 K are presented in Fig. 4a (zeolites Zn(*x*)NaY) and Fig. 4b (zeolites Na(*x*)HY). On acid zeolites, the pyridinium ion (pyridine adsorbed on Brønsted acid sites) shows absorption bands at 1540, 1480–1500 and 1640 cm^{-1} [18, 19]. Pyridine coordinatively bonded on Lewis acid sites gives rise to characteristics bands at 1440–1460, 1480–1500 and 1600 cm^{-1}. The 1600 cm^{-1} band is the

Table 2 Characterization of sample acidity: TPD of NH_3 and FTIR of pyridine

Samples	TPD of NH_3	FTIR of pyridine					
	Total acid site density	T = 423 K[a]			T = 573 K[a]		
	(μmol/g)	L (area/g)	B (area/g)	L/(L + B)	L (area/g)	B (area/g)	L/(L + B)
NaY	280	525	–	1	181	–	1
Zn(2.4)NaY	976	624	10	0.99	209	2	0.99
Zn(5.2)NaY	1492	965	18	0.98	520	6	0.99
Zn(9.3)NaY	2121	1200	37	0.97	880	9	0.99
Na(6.0)HY	880	256	395	0.39	77	180	0.30
Na(4.9)HY	924	282	462	0.38	108	190	0.36
Na(0.3)HY	1430	465	310	0.60	177	209	0.46

[a] Evacuation temperature after adsorption of pyridine at 298 K (B: Brønsted sites; L: Lewis sites)

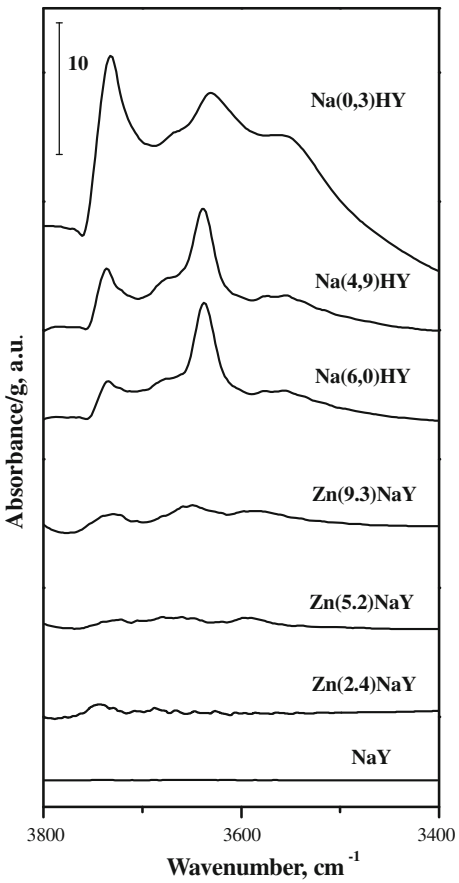

Fig. 3 FTIR spectra of the samples in the hydroxyls stretching region. Samples degassed at 773 K for 4 h

most sensitive band, that shifts to higher frequency with the increase in the strength of the acid sites [20].

The pyridine absorption spectrum on zeolite NaY in Fig. 4a did not reveal the presence of surface Brønsted sites and presented only the bands arising from pyridine adsorbed on Na^+ Lewis sites (1445 and 1600 cm^{-1}), which is consistent with the IR characterization of hydroxyl groups in Fig. 3. The addition of Zn (sample Zn(2.4)NaY) gave rise to an additional absorption band at 1455 cm^{-1} corresponding to pyridine absorbed on Zn^{+2} cations [21]. The intensity of the band 1455 cm^{-1} increased almost linearly with the Zn loading while the band at 1445 cm^{-1} simultaneously decreased because of the elimination of Na^+ cations. The replace of Na^+ by Zn^{2+} is also indicated by the disappearance of the 1600 cm^{-1} band and the development of a new sharp band at 1610 cm^{-1}. The amounts of pyridine remaining on Brønsted (B) and Lewis (L) acid sites of samples Zn(*x*)NaY after evacuation at 423 and 573 K were obtained by deconvolution and integration of pyridine absorption bands appearing at 1540 and 1440–1460 cm^{-1}, respectively. Results are given in Table 2. By comparing columns 5 and 8 in Table 2, it can be inferred that the addition of Zn generated stronger Lewis acid sites on parent NaY zeolite. Indeed, after evacuation at 573 K zeolite Zn(9.30)NaY retained 75% of the pyridine remaining after evacuation at 423 K while zeolite NaY retained only 35%. This result is consistent with those obtained by NH_3 TPD (Fig. 2a). Data of Table 2 also show that the addition of Zn generated only very small amounts of Brønsted acid sites; the L/(L + B) ratio on Zn(*x*)NaY samples was, in fact, higher than 0.97.

The IR spectra of pyridine adsorbed on zeolites Na(*x*)HY are presented in Fig. 4b. The exchange of zeolite NaY with NH_4Cl(aq.) generated Brønsted acid sites (pyridine absorption band at 1540 cm^{-1}) and a new band at 1455 cm^{-1} arising from pyridine adsorbed on Al^{3+} cations [21]. The band at 1445 cm^{-1} (pyridine adsorbed on Na^+ cations) diminished with the exchange degree. Na(*x*)HY samples presented predominantly Brønsted acidity; the L(L + B) ratios on Na(6.0)HY and Na(4.9)HY samples after evacuation at 423 K were, in fact, about 0.38 (Table 2). In contrast, the L/(L + B) ratio on Na(0.3)HY was 0.6, probably reflecting the formation of tricoordinated aluminium atoms by dehydroxylation of the zeolite. In previous work [22], it has been reported in fact that the increase of calcination temperature beyond 723 K converts Brønsted acid sites into Lewis acid sites because of elimination of hydroxyl groups and formation of tricoordinate Al atoms. Regarding the acid sites strength, Table 2 shows that after evacuation at 573 K the L(L + B) ratio decreased in comparison with the ratio values obtained after evacuation at 423 K. This result indicated the presence of strong Brønsted acid sites on Na(*x*)HY samples; in particular, sample Na(0.3)HY retained a high density of Brønsted acid sites after evacuation at 573 K (Table 2). The presence of strong acid sites on zeolites HY has been explained by considering an interaction of some bridged OH groups with the Lewis sites [23, 24].

3.2 Catalytic Results

Catalysts were tested for the gas-phase alkylation of phenol with methanol at 473 K. Main reaction products were *o*- and *p*-cresols, anisole, xylenols and methylanisoles. Anisole and cresols are primary reaction products while methylanisoles and xylenols are formed from consecutive alkylation of anisole and cresols, respectively. Scheme 1 shows a simplified reaction network, according to [15]. Figure 5 shows as an example the phenol conversion (X_P) and selectivities (S_i) obtained at 473 K for phenol methylation on Zn(9.3)NaY. Phenol conversion diminished from 39.3 to 12% after 4 h on stream, reflecting the catalyst activity decay during the run. Production of *o*- and *p*-cresol was clearly predominant, but *p*-cresol increased while *o*-cresol diminished with the progress of the reaction. The selectivity to anisole slightly increased at the expenses of

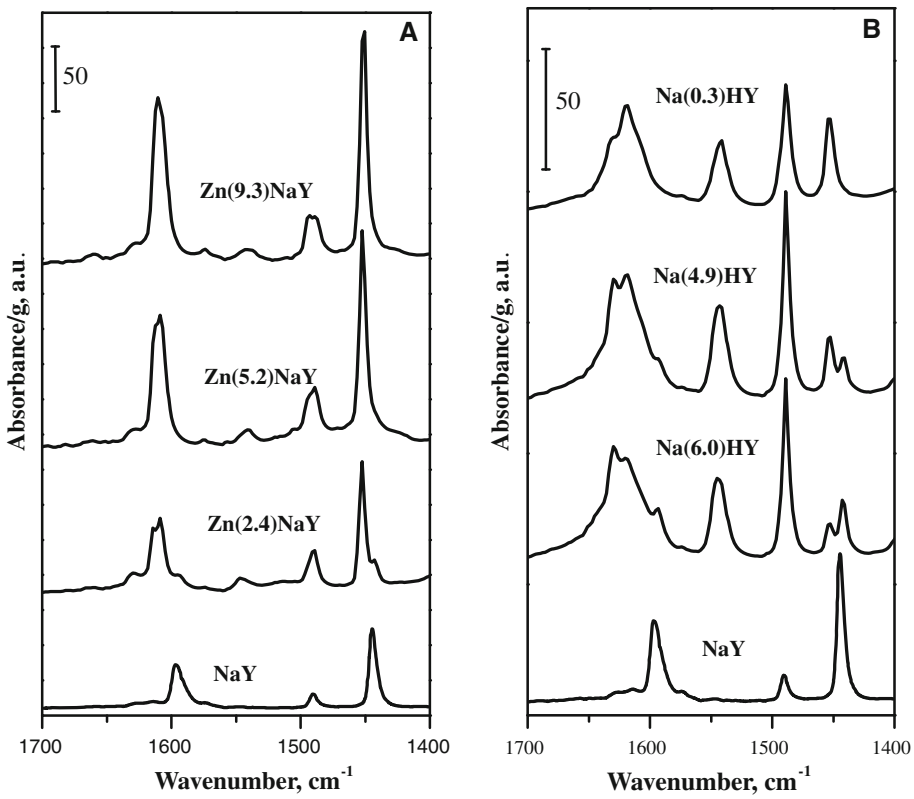

Fig. 4 FTIR spectra of pyridine adsorbed at 298 K and evacuated at 423 K on: **a** zeolites Zn(*x*)NaY; **b** zeolites Na(*x*)HY

xylenols and methylanisoles. Formation of *m*-cresol was very small (lower than 5%), but slightly increased on stream via the consecutive isomerization of *p*- and *o*-cresols, as depicted in Scheme 1.

Due to catalyst deactivation observed in Fig. 5, initial catalytic results for all the samples were obtained by extrapolation of reactant and product concentration curves to zero time-on-stream. The phenol conversions obtained at zero time and after 4 h on stream are shown in Table 3. Zeolite NaY was practically inactive at 473 K, but after its exchange with Zn^{2+} cations efficiently promoted the alkylation of phenol. In fact, the initial phenol conversion increased from 8.0% on Zn(2.4)NaY to 39.3% on Zn(9.3)NaY. Table 3 also presents the initial selectivities obtained on Zn(*x*)NaY samples. The selectivities to *o*- and *p*-cresols increased with the Zn content in the sample, reaching 34.0 and 26.2%, respectively on Zn(9.3)NaY. All the Zn(*x*)NaY samples formed preferentially the *ortho*-isomer, being the *para*-:*ortho*-cresol ratio about 0.8. The selectivity to xylenols increased with phenol conversion, which was expected taking into account that xylenols are formed via consecutive reaction pathways in the phenol alkylation reaction network (Scheme 1). In contrast, the formation of methylanisoles did not change significantly with the phenol conversion increase. This result, together with the fact that the cresols selectivity increased at the expense of anisole strongly suggested that anisole is essentially converted consecutively to cresols. The catalyst activity decay increased with the Zn loading in the sample; for example, phenol conversion was initially 39.3% on Zn(9.3)NaY but decreased to 12% after 4 h on stream (Table 3).

Regarding Na(*x*)HY samples, the exchange of Na^+ with H^+ activated the parent NaY zeolite for phenol alkylation

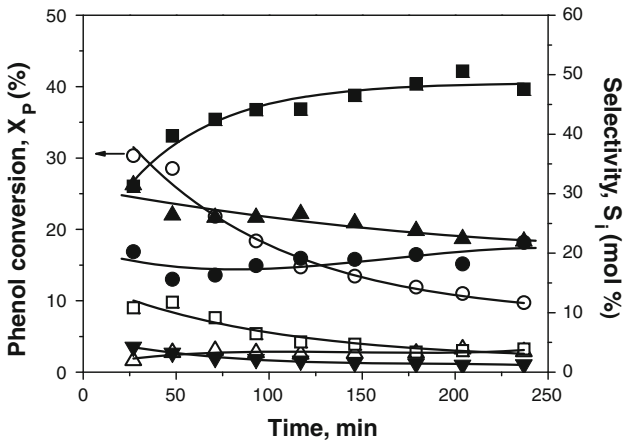

Fig. 5 Phenol conversion (X_P) and selectivities as a function of time-on-stream on Zn(9.3)NaY (473 K, 101.3 kPa total pressure, $W/F_P^0 = 112$ g h/mol, M/P = 2) (*filled square*) *p*-cresol (*filled triangle*) *o*-cresol, (*filled circle*) anisole, (*open square*) Xylenols, (*filled inverted triangle*) methylanisoles, (*open triangle*) *m*-cresol

Table 3 Catalyst activity, selectivity and stability for the gas-phase alkylation of phenol with methanol

Catalyst	Phenol conversion Xp (%)		Methanol conversion, X_M (%)	Selectivities at $t = 0$ S_i^0 (%)						Initial catalyst deactivation
	$t = 0$	$t = 4$ h	$t = 4$ h	Anisole	*o*-Cresol	*p*-Cresol	*m*-Cresol	Xylenols	Methylanisoles	$d_0 \times 10^3$ (h^{-1})[a]
NaY	0.3	0	10.0	–	–	–	–	–	–	–
Zn(2.4)NaY	8.0	9.0	11.2	60.0	22.0	18.0	–	–	–	0.2
Zn(5.2)NaY	19.4	12.0	14.3	45.0	25.0	20.0	3.5	2.5	4.0	2.5
Zn(9.3)NaY	39.3	12.0	15.1	20.7	34.0	26.2	2.3	13.5	3.3	8.2
Na(6.0)HY	23.0	9.2	20.4	55.2	22.5	12.5	3.3	2.4	4.1	2.5
Na(4.9)HY	25.0	6.0	25.3	50.5	25.6	14.4	1.3	2.4	5.8	5.9
Na(0.3)HY	73.0	0	44.4	0.5	16.5	26.3	12.9	43.8	0	26.2

T = 473 K, M/P = 2, $N_2/(M + P) = 26.8$

[a] Determined from the deactivation curves of Fig. 6 as: $d_0 = -(da_P/dt)_{t=0}$

(Table 3). Phenol conversion was 23.0% on Na(6.0)HY forming 55.2% of anisole and 38.3% of cresols. At similar conversion levels, Na(6.0)HY formed more anisole and less cresols than Zn(5.2)NaY. The initial *para*-:*ortho*-cresol ratio on Na(6.0)HY and Na(4.9)HY was about 0.56. Sample Na(0.3)HY was highly active ($X_P^0 = 73\%$) and anisole was completely converted to *o*- and *p*-cresols that in turn formed significant amounts of xylenols ($S_{Xyl}^0 = 43.8\%$). Formation of *p*-cresol was predominant on Na(0.3)HY (the *para*-:*ortho*-cresol ratio was 1.6). The initial *m*-cresol selectivity increased because of the high activity of sample Na(0.3)HY that promoted the *m*-cresol formation from consecutive isomerization of *o*- and *p*-cresols (Scheme 1). All the Na(*x*)HY samples deactivated on stream; in particular, phenol conversion on Na(0.3)HY was negligible after 2 h on stream.

3.3 Catalytic Performance and Surface Acid Properties

Zeolite NaY that contains only weak and medium Lewis acid sites was inactive for phenol methylation at 473 K. The exchange of Na^+ with Zn^{+2} generated strong Lewis acid sites that efficiently catalyzed the reaction, being phenol conversion almost proportional to the Zn loading (Tables 2, 3). This result showed that the reactants, phenol and methanol, are activated on strong Lewis acid sites forming the primary products derived from *O*-alkylation (anisole) and *C*-alkylation (*p*- and *o*-cresol) reactions. Anisole was predominantly formed at low phenol conversion levels (sample Zn(2.4)NaY in Table 3), indicating that strong Lewis acid sites may strongly interact with the aromatic ring and adsorb phenol in a planar position thereby liberating the oxygen of the hydroxyl group for the attack of the alkylating agent formed from methanol on adjacent surface acid sites. Nevertheless, formation of *p*- and *o*-cresols from anisole increased with increasing catalyst activity; thus, for $X_P^0 = 39.3\%$ (sample Zn(9.3)NaY in Table 3) the selectivity to cresol isomers was substantially higher in comparison to anisole selectivity. Cresols may be formed from anisole via two reaction pathways: (i) intramolecular rearrangement of anisole, or (ii) alkylation of phenol with anisole. Previous studies [10, 25, 26] have specifically reported that on solid acids anisole produces cresols by alkylating phenol, probably reflecting that anisole is a more effective alkylating agent than methanol [27]. This late reaction is efficiently promoted on zeolites BEA containing a high density of Lewis acid sites [26], which is consistent with the results observed here in Table 3.

Zeolite NaY also became active for phenol methylation at 473 K after exchanging with NH_4Cl(aq.). The replacement of Na^+ with H^+ cations generated Brønsted acid sites and also decreased the density of Lewis acid sites because of the elimination of Na^+ cations, although simultaneously a number of Al^{3+} sites became accessible to reactant adsorption (Figs. 3, 4b; Table 2). Phenol conversion was 23% on Na(6.0)HY; a similar phenol conversion value was obtained on Zn(5.2)NaY (Table 3). However, the product distributions on Zn(5.2)NaY and Na(6.0)HY were different; for example the ratios between anisole and cresols (*ortho* and *para*-isomers) on Zn(5.2)NaY and Na(6.0)HY were 1.0 and 1.6, respectively. The higher selectivity to anisole on Na(6.0)HY probably reflects the generation of Brønsted acid sites on this zeolite. In fact, previous works have reported that Brønsted solid acids, such as HPA/SiO_2 or resin Nafion-H, form predominantly anisole [11, 15]. The lower selectivity to anisole observed on Zn(5.2)NaY as compared to Na(6.0)HY also explains that the *p*-cresol/*o*-cresol ratio is higher on Zn(5.2)NaY because the consecutive conversion of anisole to cresols produces mainly *p*-cresol [26]. The product distribution on Na(4.9)HY was similar to that observed on Na(6.0)HY (Table 3). In contrast, sample Na(0.3)HY was very active ($X_P^0 = 73\%$) and converted almost completely anisole to xylenols and cresol

isomers. This result reflects essentially the presence of strong Brønsted acid sites on Na(0.3)HY (Figs. 2b, 3) that promote alkylation and isomerization reactions. In particular, significant amounts of *m*-cresol were formed on Na(0.3)HY from *p*- and *o*-cresol isomerizations.

3.4 Catalyst Deactivation

All the samples used in this work deactivated on stream. In Fig. 6 we have plotted the evolution of the activity for the conversion of phenol (a_P) as a function of time on stream. The activity a_P is defined as $a_P = r_P/r_P^0$, where r_P and r_P^0 are the rates of phenol conversion at times t and zero, respectively. From the curves of Fig. 6 we calculated the initial deactivation rate (d_0, min^{-1}) as the initial slope of the curves, i.e., $d_0 = -(da_P)/dt)_{t=0}$; the obtained d_0 values are listed in the Table 3.

Data in Fig. 6 and Table 3 show that the activity decay on zeolites Zn(*x*)NaY increased with the sample Zn content. For example, the initial deactivation d_0 increased from 0.2 min^{-1} on Zn(2.4)NaY to 8.2 min^{-1} on Zn(9.3)NaY (Table 3). The activity decay also increased with the exchange degree on zeolites Na(*x*)HY. In particular, Na(0.3)HY rapidly deactivated with the progress of the reaction and lost completely the ability for alkylating phenol after 2 h on stream (Fig. 6); the d_0 value on Na(0.3)HY was 26.2 min^{-1}. As a general remark, it has to be noted in Table 3 that the catalyst deactivation increased with phenol conversion: the higher X_P^0, the higher d_0.

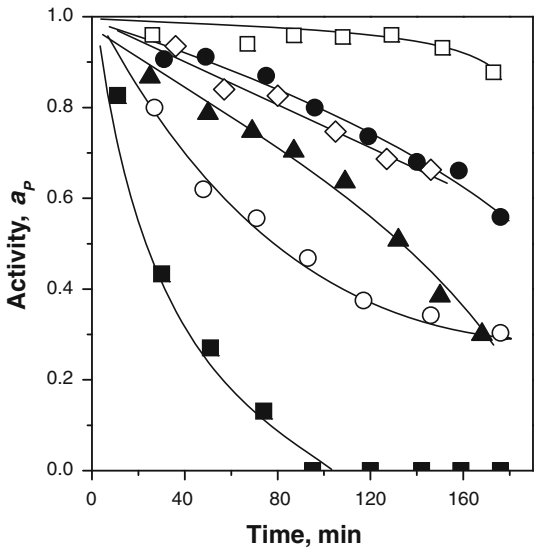

Fig. 6 Catalyst deactivation: Activity for phenol conversion (a_P) as a function of time on stream (reaction conditions as in Fig. 5) (*open square*) Zn(2.4)NaY, (*open diamond*) Zn(5.2)NaY, (*open circle*) Zn(9.3)NaY, (*filled circle*) Na(6.0)HY, (*filled triangle*) Na(4.9)HY, (*filled square*) Na(0.3)HY

Previous work has shown that coke formation reactions are responsible for the deactivation of acid zeolites during alkylation reactions [28]. In particular, the dehydration and condensation of two molecules of methanol giving DME leads usually to the formation of carbonaceous deposits on solid acids because DME is easily converted to hydrocarbons such as methane, ethene, propane, propene, butenes and aromatics [29]. In all our catalytic runs we detected DME and hydrocarbons, thereby suggesting that the self-oligomerisation-cyclisation of methanol to olefins and aromatics contributes to the observed catalyst activity decay. Formation of hydrocarbons from methanol is particularly promoted on strong acid sites that dehydrate methanol forming reactive methoxy intermediates for hydrocarbon formation [30]. Anisole dealkylation that forms phenol and olefins also leads to the formation of coke [26]; however, this reaction is not favored in phenol methylation because phenol is one of the reactants. Formation of heavy dialkylated products, in particular xylenols, may also form carbonaceous products and contribute to catalyst deactivation. Indeed, the retention of polyalkylated phenols has been proposed as one of the mechanism responsible for the progressive deactivation of the catalyst in the methylation of phenol [13]. The observed correlation in Table 3 between X_P^0 and d_0 suggests in fact that the catalyst activity decay increases with the formation of heavier secondary products at high conversion levels.

4 Conclusions

Zeolite NaY contains only weak and medium Lewis acid sites and is inactive for promoting the gas-phase alkylation of phenol with methanol at 473 K. However, after its exchange with Zn^{2+} (samples Zn(*x*)NaY) or H^+ (samples Na(*x*)HY) cations efficiently catalyzes the phenol methylation reaction. The addition of Zn^{+2} generates essentially strong Lewis acid sites that activate the reactants, phenol and methanol, and form the primary products derived from *O*-alkylation (anisole) and *C*-alkylation (*p*- and *o*-cresol) reactions. Phenol conversion increases almost linearly with the Zn content on the sample, and as a consequence, increases the formation of secondary products via consecutive reaction pathways, in particular xylenols, mainly at the expense of anisole. The exchange of zeolite NaY with H^+ generates Brønsted acid sites and diminishes the density of Lewis acid sites. Thus, zeolites Na(*x*)HY present predominantly Brønsted acidity that initially promotes the preferential formation of anisole and the *ortho*-selectivity, producing more *o*-cresol than *p*-cresol. The complete exchange of zeolite NaY with H^+ leads to the formation of HY zeolites containing strong Brønsted acid sites that are very active for phenol methylation but produce mainly

dialkylated compounds such as xylenols. All the Zn(x)NaY and Na(x)HY samples deactivate on stream due to coke formation, but the zeolite activity decay increases with the exchange degree, probably because of the concomitant increase of the sample acidity.

Acknowledgments This work was supported by the Universidad Nacional del Litoral (UNL), Consejo Nacional de Investigaciones Científicas y Técnicas (CONICET), and Agencia Nacional de Promoción Científica y Tecnológica (ANPCyT), Argentina.

References

1. Bailey JE, Bohnet M, Brinker J (eds) (1988) Ullman's encyclopedia of industrial chemistry, 6th edn. Willey-VCH, Weinheim
2. Devassy BM, Shanbag GV, Lefebvre F, Halligudi SB (2004) J Mol Catal A: Chem 210:125
3. Sarish S, Devassy BM, Halligudi SB (2005) J Mol Catal A: Chem 235:44
4. Landau MV, Kaliya ML, Herskowitz M (2001) Appl Catal A: General 208:21
5. Tanabe K, Hölderich WF (1999) Appl Catal A: General 181:399
6. Velu S, Swamy CS (1994) Appl Catal A: General 119:41
7. Balsama S, Beltrame P, Beltrame PL, Carniti P, Forni L, Zuretti G (1984) Appl Catal 13:161
8. Renaud M, Chantal P, Kaliaguine S (1986) Can J Chem Eng 64:787
9. Marczewski M, Perot G, Guisnet M (1988) In Guisnet M, Barrault J, Bouchoule C, Duprez D, Montassier C, Pérot G (eds) Studies in surface science and catalysis, vol. 41, p 273. Elsevier, Amsterdam
10. Marczewski M, Bodibo JP, Perot G, Guisnet M (1989) J Molec Catal 50:211
11. Santacesaria E, Grasso D, Gelosa D, Carrá S (1990) Appl Catal 64:83
12. Tanabe K, Nishizaki T (1977) In: Bond GC, Wells PB and Tompkins FC (eds) Proc 6th Int Congr Catal, vol. 2, p. 863. The Chemical Society, London
13. Bregolato M, Bolis V, Busco C, Ugliengo P, Bordiga S, Cavani F, Ballarini N, Maselli L, Paseri S, Rossetti I., Forni L (2007) J Catal 245:283
14. Bhattacharyya KG, Talukdar AK, Das P, Sivasanker S (2003) J Molec Catal 197:255
15. Sad ME, Padró CL, Apesteguía CR (2008) Catal Today 133–135: 720
16. Boréave A, Auroux A, Guimon C (1997) Microp Mat 11:275
17. Padró CL, Apesteguía CR (2004) J Catal 226:308
18. Parry EP (1963) J Catal 2:371
19. Knözinger H (1976) Adv Catal 25:184
20. Busca G (1998) Catal Today 41:19
21. Penzien J, Abraham A, van Bokhoven J, Jentys A, Müller T, Sievers C, Lercher JJ (2004) J Phys Chem B 108:4116
22. Ward JW (1967) J Catal 9:225
23. Beyerlien RA, Mc Vicker GB, Yacullo LN, Ziemak JJ (1988) J Phys Chem 92:1967
24. Corma A, Fornes F, Rey F (1990) Appl Catal 59:267
25. Beltrame P, Beltrame PL, Carniti P, Castelli A, Forni L (1987) Appl Catal 29:327
26. Sad ME, Padró CL, Apesteguía CR (2010) J Mol Catal A: Chemical 327:63
27. Kaspi J, Olah GA (1978) J Org Chem 43:3142
28. Bjørgen M, Olsbye U, Kolboe S (2003) J Catal 215:30
29. Dahl IM, Kolboe S (1994) J Catal 149:458
30. Tsoncheva T, Dimitrova R (2002) Appl Catal A: Gen 225:101